SUPPLEMENTARY FIGURES

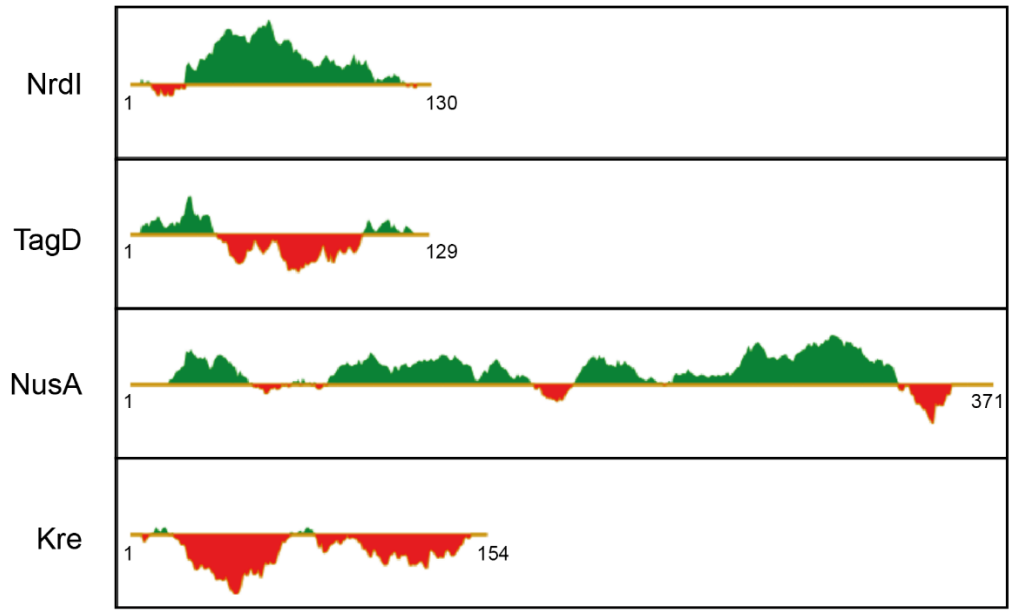

Figure S1. **Predicted foldedness of selected model proteins**.

FoldIndex (Prilusky et al., 2005) analysis of *B. subtilis* proteins used in mSA-fusion constructs. Structurally ordered sequences (green) and disordered regions (red) are highlighted. The selected proteins include: NrdI (a flavodoxin-like protein component of ribonucleoside reductases) (Cotruvo and Stubbe, 2010), TagD (glycerol-3-phosphate cytidyltranferase involved in teichoic acid synthesis) (Park et al., 1993), NusA (transcription factor involved in pausing/termination) (Gusarov and Nudler, 2001) and Kre (also known as YkyB, a regulator of the competence transcription factor ComK) (Gamba et al., 2015). PDB structures are available for *B. subtilis* NrdI bound to riboflavin monophosphate (PDB: 1RLJ); *B. subtilis* TagD dimer bound to cytidine-5'-triphosphate (PDB: 1COZ); *Thermotoga maritima* NusA, which has 51% identity to *B. subtilis* NusA (PDB: 1HH2).

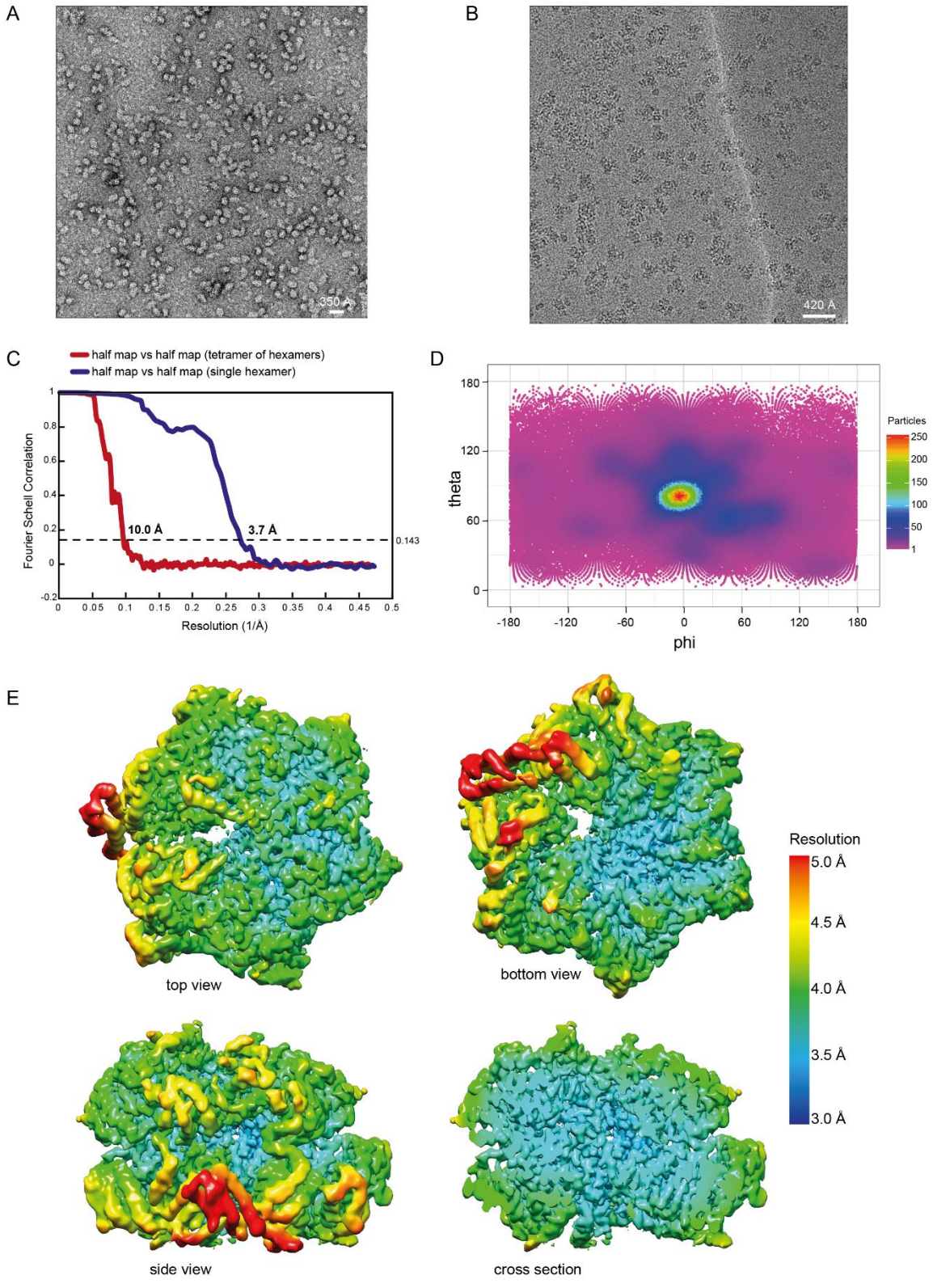

Figure S2. EM analysis of *B. subtilis* ClpC$_{DWB}$.

(**A**) Negative stain EM analysis of *B. subtilis* ClpC$_{DWB}$ in the absence of BacPROTAC-1: representative micrograph from the 1,004 collected (scale bar = 350 Å). (**B**) Cryo-EM analysis of *B. subtilis* ClpC$_{DWB}$ in the presence of BacPROTAC-1: a representative

micrograph from the 4,455 collected (scale bar = 420 Å). (**C**) FSC curves of the final maps obtained by cryo-EM analysis, showing a resolution of 10 Å for the tetramer of hexamers map and 3.7 Å for the single hexamer map. (**D**) Angular distribution of the particles used to reconstruct the single hexamer map. (**E**) Local resolution map for the single hexamer in different orientations.

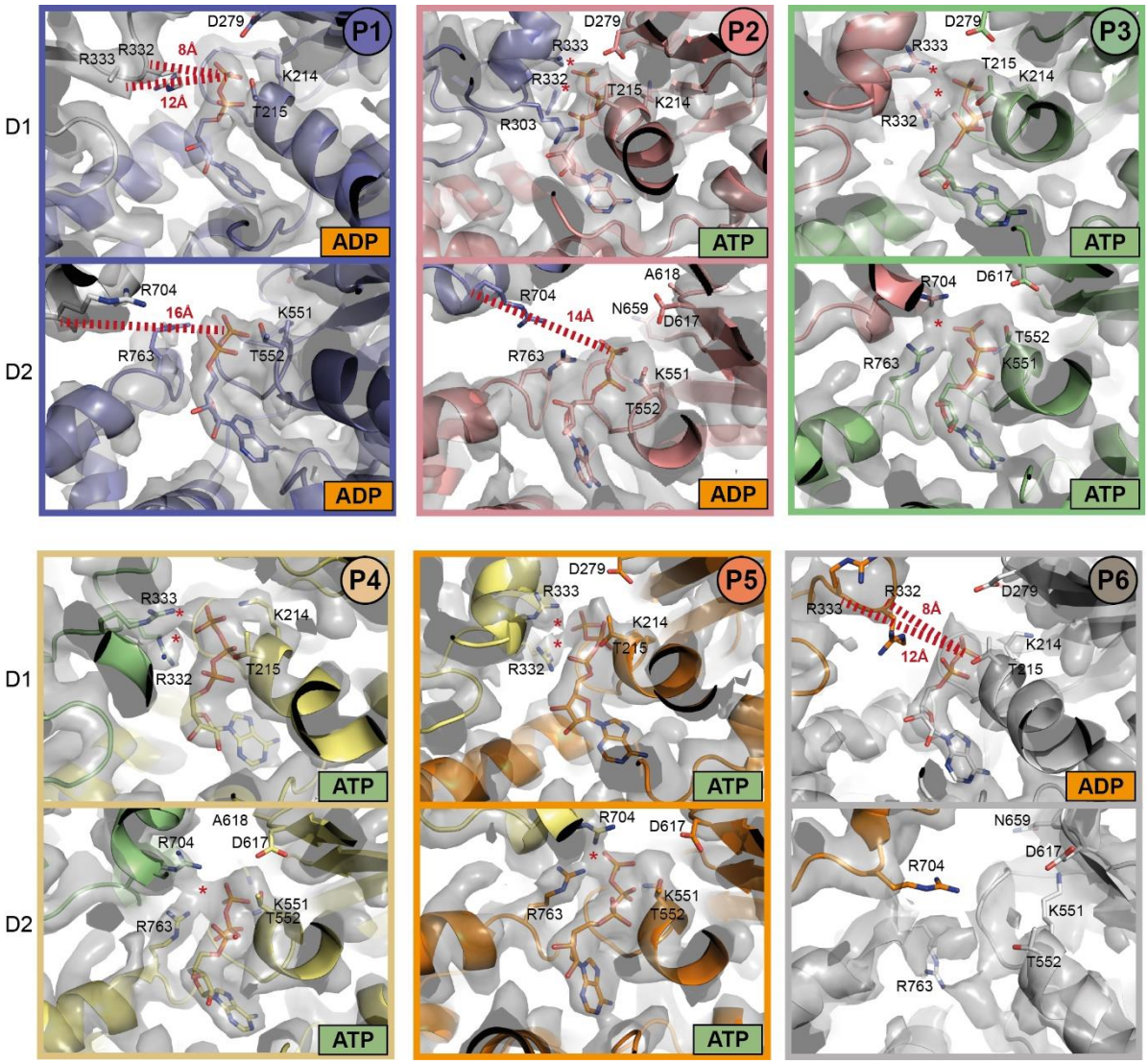

Figure S3. Nucleotide binding sites of the six ClpC$_{DWB}$ protomers.

The different panels show the modelled nucleotide in each active site pocket and some of the crucial residues involved in ATP hydrolysis and ATP/ADP interaction. Contacts between ATP γ-phosphate and Arg fingers in D1 (R332-R333) and D2 (R704) are indicated (*) for the ATP-bound sites, while distances between Arg fingers Cα and ADP β-phosphate are shown for ADP-bound sites. The cryo-EM map is represented as grey surface around the modelled protein structure.

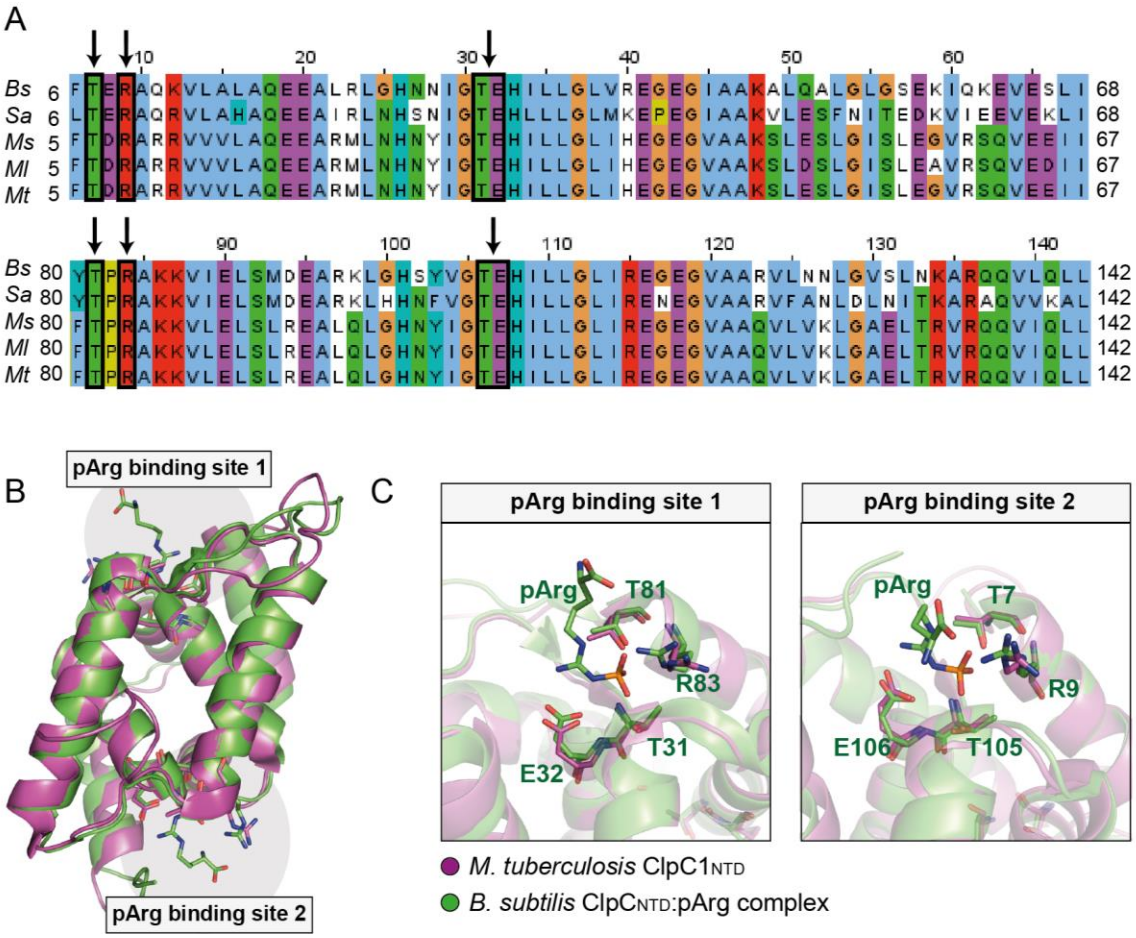

Figure S4. Conservation of pArg binding sites in Gram-positive bacteria and mycobacteria.

(**A**) Sequence alignment of ClpC$_{NTDs}$ from different species (*B. subtilis*, *S. aureus*, *M. smegmatis*, *M. leprae*, *M. tuberculosis*). Residues interacting with pArg are circled in black and marked by an arrow. (**B**) Structure of pArg-bound *B. subtilis* ClpC$_{NTD}$ (colored green, PDB: 5HBN) superposed with *M. tuberculosis* ClpC1$_{NTD}$ (colored magenta, PDB: 3WDB). (**C**) Zoomed view of the two pArg binding sites shows that crucial residues interacting with the phospho-guanidino group are conserved in *M. tuberculosis*.

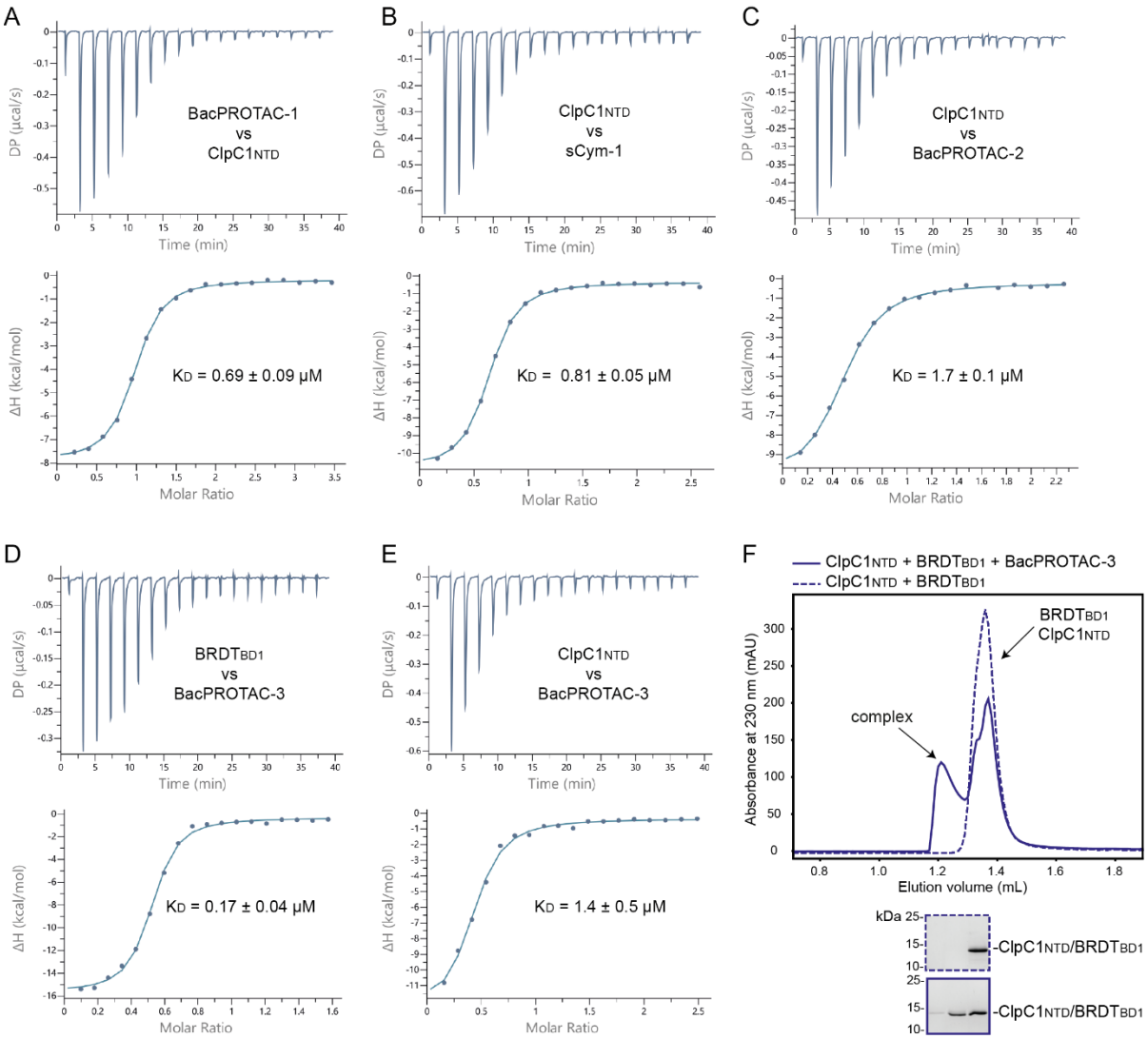

Figure S5. Characterization of compounds and BacPROTACs binding ClpC1$_{NTD}$.

(**A**) Representative ITC titration of BacPROTAC-1 (400 µM loaded in the syringe) against ClpC1$_{NTD}$ (22 µM loaded in the cell); reported K_D value represents the average ± standard deviation of three independent measurements. (**B**) Representative ITC titration of ClpC1$_{NTD}$ (406 µM loaded in the syringe) against sCym-1 (30 µM loaded in the cell), reported K_D value represents the average ± standard deviation of three independent measurements. (**C**) Representative ITC titration of ClpC1$_{NTD}$ (356 µM loaded in the syringe) against BacPROTAC-2 (30 µM loaded in the cell), reported K_D value represents the average ± standard deviation of two independent measurements. (**D**) Representative ITC titration of BRDT$_{BD1}$ (124 µM loaded in the syringe) against BacPROTAC-3 (15 µM loaded in the cell); reported K_D value represents the average ± standard deviation of three independent measurements. (**E**) Representative ITC titration of ClpC1$_{NTD}$ (392 µM loaded in the syringe) against BacPROTAC-3 (30 µM

loaded in the cell); reported K_D value represents the average ± standard deviation of five independent measurements. (**F**) SEC analysis of a stoichiometric $BRDT_{BD1}$:$ClpC1_{NTD}$ mixture in the presence (solid line) or absence (dashed line) of BacPROTAC-3. The two proteins elute at the same volume also in the absence of BacPROTAC because of their similar size, however BacPROTAC-3 addition mediates formation of an additional peak compatible with the elution volume expected for the $BRDT_{BD1}$:BacPROTAC-3:$ClpC1_{NTD}$ ternary complex. Coomassie stained SDS-PAGE gel of the collected peak fractions is shown. $BRDT_{BD1}$ and $ClpC1_{NTD}$ have identical electrophoretic mobility and are thus not distinguishable on the Coomassie stained gel.

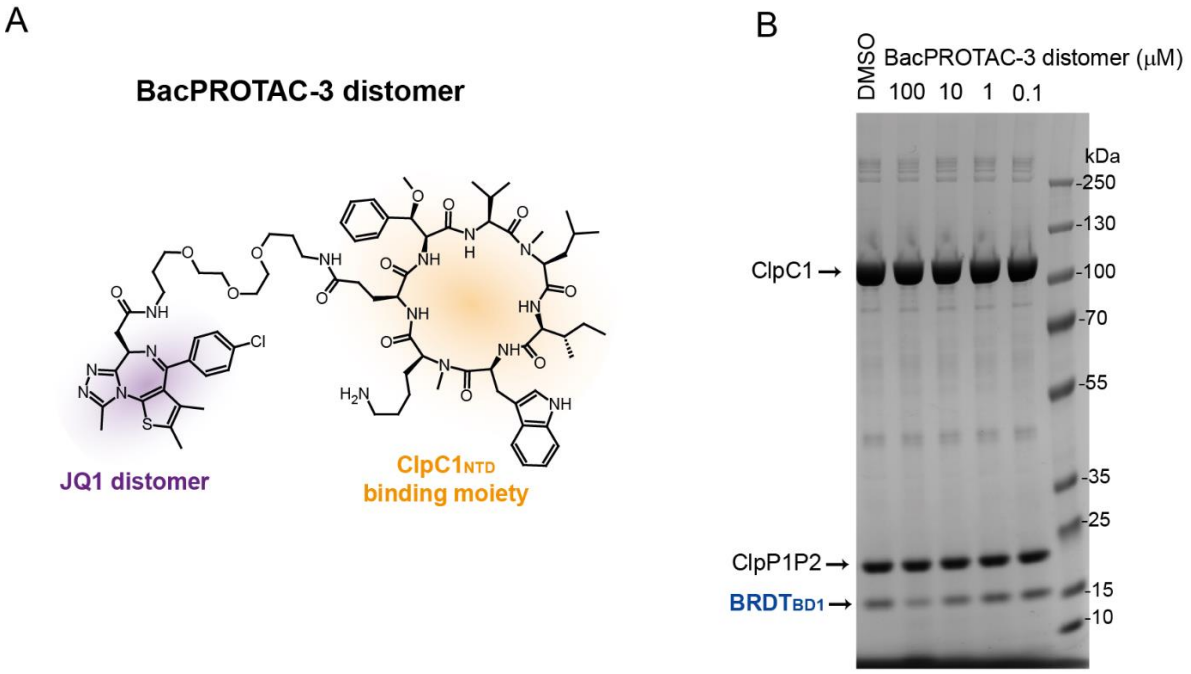

Figure S6. BacPROTAC-3-induced degradation is stereospecific.

JQ1 binding to $BRDT_{BD1}$ is stereo-specific (Filippakopoulos et al., 2010). Only the JQ1-(*S)* enantiomer is active (eutomer), while the JQ1-(*R)* enantiomer binds with an approximately 60-fold lower affinity (distomer). (**A**) Chemical structure of the BacPROTAC-3 distomer, synthesized using JQ1-(*R).* (**B**) *In vitro* degradation assay using *M. smegmatis* ClpC1P1P2 analyzed after 2 hours incubation showing that $BRDT_{BD1}$ not significantly degraded in presence of 100-0.1 μM BacPROTAC-3 distomer, in contrast to the BacPROTAC-3 eutomer (**Figure 5B**).

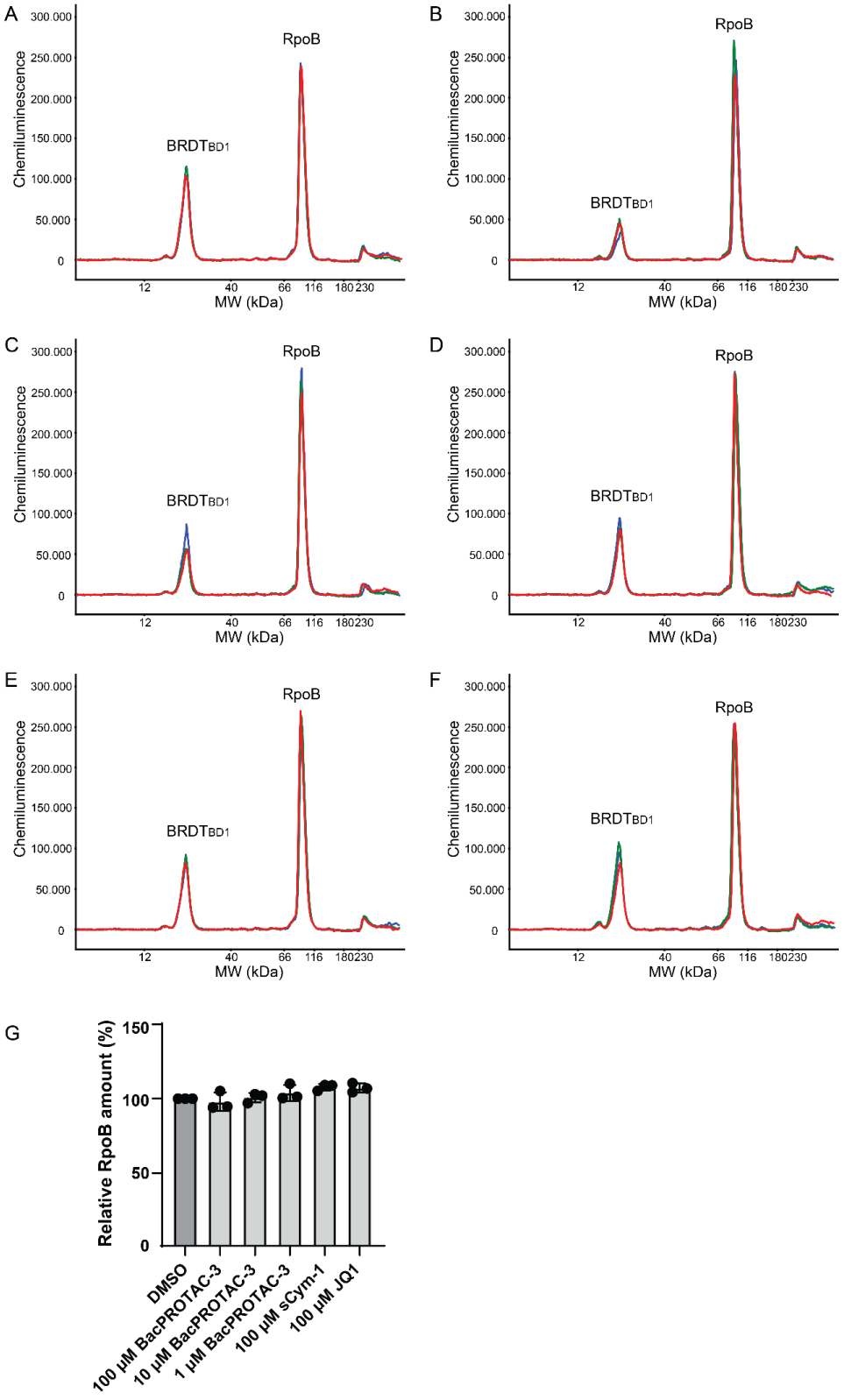

Figure S7. $BRDT_{BD1}$ levels detected by capillary Western blot upon BacPROTAC treatment of *M. smegmatis* cells.

Electropherograms showing intensity of the chemiluminescent signal plotted against the apparent molecular weight detected using anti-BRDT and anti-RpoB antibodies.

(**A-F**) Detected peaks for lysates of a *M. smegmatis* culture expressing $BRDT_{BD1}$ after each treatment (30 minutes) in triplicate: (**A**) DMSO, (**B**) 100 µM BacPROTAC-3, (**C**) 10 µM BacPROTAC-3, (**D**) 1 µM BacPROTAC-3, (**E**) 100 µM sCym-1, (**F**) 100 µM JQ1. (**G**) Bar chart showing quantification of detected RpoB peaks (loading control) from three independent experiments normalized to DMSO treatment (dark grey bar) and plotted as mean ± standard deviation. Quantification of the $BRDT_{BD1}$ peak is shown in **Figure 5D**.

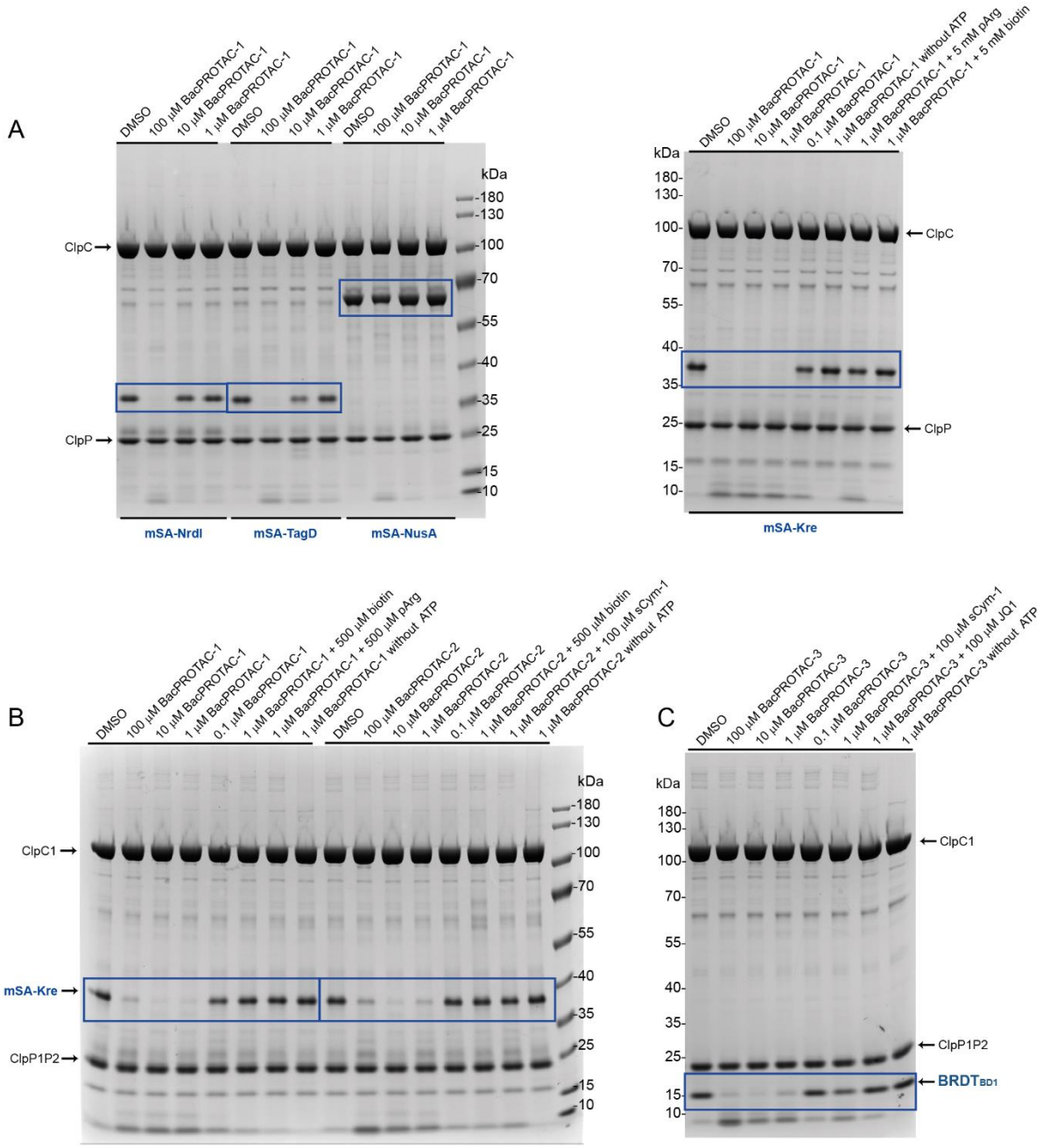

Figure S8. Uncropped assay gels. Uncropped Coomassie stained SDS-PAGE gels shown in (**A**) **Figure 1G** and **1H**; (**B**) **Figure 4B** and **4H**; (**C**) **Figure 5B**.

SUPPLEMENTARY TABLES

Table S1: Crystallographic analysis of ClpC1$_{NTD}$:sCym-1 complex. Data collection and refinement statistics

PDB ID	7AA4
Space group	*P*1
Cell dimensions	
a, *b*, *c* (Å)	31.35, 33.68, 35.81
α, *β*, *γ* (°)	86.178, 94.216, 103.176
Resolution (Å)[a,b]	25 – 1.68 (1.72 – 1.68)
$R_{meas(I)}$	0.062 (0.112)
I/σ (I)	22.6 (12.5)
$CC_{1/2}$	0.998 (0.992)
Completeness (%)	93.8 (86.5)
Redundancy	5.8 (5.4)
Resolution (Å)	25 – 1.68
No. reflections	15,165
R_{work} / R_{free}	17.0 / 20.3
No. atoms	
protein	1254
ligand	66
water	192
B factors	
protein	11.9
ligand	13.5
water	23.0

R.m.s. deviations	
Bond lengths (Å)	0.006
Bond angles (°)	0.789

[a]Values in parentheses are for highest-resolution shell.

[b]Due to experimental constraints the resolution needed to be truncated to this resolution.

Table S2. Amino acid sequences of mSA fusion proteins.

Construct name	Amino acid sequence
mSA	MHHHHHHSSGVDLGTENLYFQSSQDLASAEAGITGTWYNQSGSTFTVTAGAD GNLTGQYENRAQGTGCQNSPYTLTGRYNGTKLEWRVEWNNSTENCHSRTEW RGQYQGGAEARINTQWNLTYEGGSGPATEQGQDTFTKVKPSAASGSGSGSGS GS
mSA-Kre	MHHHHHHSSGVDLGTENLYFQSSQDLASAEAGITGTWYNQSGSTFTVTAGAD GNLTGQYENRAQGTGCQNSPYTLTGRYNGTKLEWRVEWNNSTENCHSRTEW RGQYQGGAEARINTQWNLTYEGGSGPATEQGQDTFTKVKPSAASGSGSGSGS MDDHAYTKDLQPTVENLSKAVYTVNRHAKTAPNPKYLYLLKKRALQKLVKEGKG KKIGLHFSKNPRFSQQQSDVLISIGDYYFHMPPTKEDFEHLPHLGTLNQSYRNP KAQMSLTKAKHLLQEYVGMKEKPLVPNRQQPAYHKPVFKKLGESYF
mSA-Kre (Cryo-EM structure determination)	MSQDLASAEAGITGTWYNQSGSTFTVTAGADGNLTGQYENRAQGTGCQNSPY TLTGRYNGTKLEWRVEWNNSTENCHSRTEWRGQYQGGAEARINTQWNLTYE GGSGPATEQGQDTFTKVKPSAASGSGSGSGSGSGSGSGSGSDDHAYTKDLQ PTVENLSKAVYTVNRHAKTAPNPKYLYLLKKRALQKLVKEGKGKKIGLHFSKNP RFSQQQSDVLISIGDYYFHMPPTKEDFEHLPHLGTLNQSYRNPKAQMSLTKAKH LLQEYVGMKEKPLVPNRQQPAYHKPVFK KLGESYFHHHHHH
mSA-NrdI	MHHHHHHSSGVDLGTENLYFQSSQDLASAEAGITGTWYNQSGSTFTVTAGAD GNLTGQYENRAQGTGCQNSPYTLTGRYNGTKLEWRVEWNNSTENCHSRTEW RGQYQGGAEARINTQWNLTYEGGSGPATEQGQDTFTKVKPSAASGSGSGSGS GSVVQIIFDSKTGNVQRFVNKTGFQQIRKVDEMDHVDTPFVLVTYTTNFGQVPA STQSFLEKYAHLLLGVAASGNKVWGDNFAKSADTISRQYQVPILHKFELSGTSK DVELFTQEVERVVTKSSAKMDPVK
mSA-TagD	MHHHHHHSSGVDLGTENLYFQSSQDLASAEAGITGTWYNQSGSTFTVTAGAD GNLTGQYENRAQGTGCQNSPYTLTGRYNGTKLEWRVEWNNSTENCHSRTEW RGQYQGGAEARINTQWNLTYEGGSGPATEQGQDTFTKVKPSAASGSGSGSGS GSMKKVITYGTFDLLHWGHIKLLERAKQLGDYLVVAISTDEFNLQKQKKAYHSYE HRKLILETIRYVDEVIPEKNWEQKKQDIIDHNIDVFVMGDDWEGKFDFLKDQCEV VYLPRTEGISTTKIKEEIAGL
mSA-NusA	MHHHHHHSSGVDLGTENLYFQSSQDLASAEAGITGTWYNQSGSTFTVTAGAD GNLTGQYENRAQGTGCQNSPYTLTGRYNGTKLEWRVEWNNSTENCHSRTEW RGQYQGGAEARINTQWNLTYEGGSGPATEQGQDTFTKVKPSAASGSGSGSGS GSMSSELLDALTILEKEKGISKEIIIEAIEAALISAYKRNFNQAQNVRVDLNRETGSI RVFARKDVVDEVYDQRLEISIEEAQGIHPEYMVGDVVEIEVTPKDFGRIAAQTAK

	QVVTQRVREAERGVIYSEFIDREEDIMTGIVQRLDNKFIYVSLGKIEALLPVNEQM PNESYKPHDRIKVYITKVEKTTKGPQIYVSRTHPGLLKRLFEIEVPEIYDGTVELKS VAREAGDRSKISVRTDDPDVDPVGSCVGPKGQRVQAIVNELKGEKIDIVNWSSD PVEFVANALSPSKVLDVIVNEEEKATTVIVPDYQLSLAIGKRGQNARLAAKLTGW KIDIKSETDARELGIYPRELEEDDEPLFTEPETAESDE

Movie S1. Cryo-EM structure of activated ClpC in complex with substrate.

The movie shows the map of the tetramer of ClpC hexamers (10 Å) and the map obtained refining a single ClpC hexamer (3.7 Å). Both maps are colored by ClpC protomer. Continuous density is observed for a substrate peptide (colored yellow) along the ClpC channel, surrounded by Tyr-containing pore loops, as described in the main text.

REFERENCES

Cotruvo, J.A., Jr., and Stubbe, J. (2010). An active dimanganese(III)-tyrosyl radical cofactor in Escherichia coli class Ib ribonucleotide reductase. Biochemistry *49*, 1297-1309.

Filippakopoulos, P., Qi, J., Picaud, S., Shen, Y., Smith, W.B., Fedorov, O., Morse, E.M., Keates, T., Hickman, T.T., Felletar, I.*, et al.* (2010). Selective inhibition of BET bromodomains. Nature *468*, 1067-1073.

Gamba, P., Jonker, M.J., and Hamoen, L.W. (2015). A Novel Feedback Loop That Controls Bimodal Expression of Genetic Competence. PLoS Genet *11*, e1005047.

Gusarov, I., and Nudler, E. (2001). Control of intrinsic transcription termination by N and NusA: the basic mechanisms. Cell *107*, 437-449.

Hofmann, F.T., Lindemann, C., Salia, H., Adamitzki, P., Karanicolas, J., and Seebeck, F.P. (2011). A phosphoarginine containing peptide as an artificial SH2 ligand. Chem Commun (Camb) *47*, 10335-10337.

Park, Y.S., Sweitzer, T.D., Dixon, J.E., and Kent, C. (1993). Expression, purification, and characterization of CTP:glycerol-3-phosphate cytidylyltransferase from Bacillus subtilis. J Biol Chem *268*, 16648-16654.

Prilusky, J., Felder, C.E., Zeev-Ben-Mordehai, T., Rydberg, E.H., Man, O., Beckmann, J.S., Silman, I., and Sussman, J.L. (2005). FoldIndex: a simple tool to predict whether a given protein sequence is intrinsically unfolded. Bioinformatics *21*, 3435-3438.